Eur Biophys J (1997) 26: 247–252

ARTICLE

P. Mazeron · S. Muller · H. El Azouzi

On intensity reinforcements in small-angle light scattering patterns of erythrocytes under shear

Received: 25 November 1996 / Accepted: 19 April 1997

Abstract On small-angle light scattering patterns obtained with erythrocytes under shear, intensity reinforcements in rings can be noticed. Why should one be interested in them and how does one explain their presence? After examining several hypotheses, analysis shows that this is the consequence of a shape effect: The red cells under stress are not three-axis ellipsoids but rather ellipsoid-like particles whose extremities are thinned.

Key words Erythrocyte deformability · Small-angle light scattering patterns · Ellipsoids · Physical optics approximation · Anomalous diffraction

Introduction

It is well known that red blood cells (RBC) exhibit remarkable deformability. Their resting shape, a biconcave disk, can be drastically changed if a stress is applied. For example, in the Couette flow generated in a classical ektacytometer (Bessis et al. 1980), RBC can become flat elongated particles with a stationary orientation (Schmid-Schönbein and Wells 1969; Goldsmith and Marlow 1972; Fischer and Schmid-Schönbein 1977). Various theoretical models such as rigid ellipsoids (Goldsmith 1967; Goldsmith and Marlow 1967,1972; Brenner and Bungway 1971), liquid droplets (Brenner and Bungway 1971; Gauthier et al. 1972; Kline 1972; Fischer et al. 1978) and thin-shells (Brennen 1975; Guerlet et al. 1977; Barthès-Biesel 1980; Richardson 1974) have been proposed to describe this behavior. The most comprehensive model consists of an ellipsoid whose membrane is tank-treading around the cell content (Keller and Skalak 1982).

P. Mazeron (✉) · S. Muller · H. El Azouzi
Groupe Physico-Chimie des Colloïdes, LESOC, UA CNRS no 406,
Université Henri Poincaré – Nancy 1, Faculté des Sciences,
BP 239, F-54506 Vandoeuvre lès Nancy Cedex, France
(e-mail: mazeron@lesoc.u-nancy.fr; Fax: 33(0)383912532)

In order to study these shear-induced deformations, classical ektacytometry coupled with small-angle light scattering experiments has been used. Light scattering by particles is very sensitive to shape and orientation effects. The experimental patterns obtained at various shear stresses (Mazeron et al., submitted for publication in Biorheology) are sharp and rich in information. Sharp because the shear rate, grad v, is homogenous for a Couette flow; the resulting deformation and orientation distribution laws are thus definitely narrow enough, approaching monodispersity. Rich because the patterns exhibit not only a central spot, but also several more or less pronounced rings. It would be a pity to confine oneself to the central spot by merely measuring its axis ratio or an isointensity contour. The largest possible amount of information must be used to characterize the scatterers. For this purpose it is necessary to have at one's disposal a scattering theory.

No exact solution for such particle geometries exists and numerical or approximate methods are needed. Because of the large value of size parameter for RBC (up to 100), numerical methods such as the discrete dipole approximation (Draine and Flatau 1993), or the T-matrix method (Barber and Hill 1990) are for the time being intractable.

The simplest theory to approximate forward light scattering is Fraunhofer diffraction (Zahalak and Sutera 1981). In this theory, the intensity distribution of the scattered light depends only on the shape and the size of the cross-sectional area of the scatterer. This approximation is easy to use but it is not really satisfactory because it does not take into account two fundamental parameters of three-dimensional scatterers: their refractive index and their volume. For this reason, it is not safe. For example, it cannot explain why some rings on experimental patterns are open and it can lead to wrong size determinations (Streekstra et al. 1993; Ravey and Mazeron 1983).

A far more plausible approximation is the anomalous diffraction approach, based on the assumption $m-1 \ll 1$ in which m is the particle refractive index (van de Hulst 1957). In this approach, it is considered that the spatial intensity distribution results from the interference between two

wave fronts: the first one corresponding to the light that travels along the scatterer and the other one to the light that traverses the scatterer. If only the first one were considered, Fraunhofer diffraction would be obtained. The size and refractive index of the particle are taken into account in the phase shift between the two waves. Anomalous diffraction is found to be a better approximation than Fraunhofer diffraction (Streekstra et al. 1993, 1994).

A more elaborate approximation is the Physical Optics Approximation (POA) recently developed for large ellipsoids (Mazeron and Muller 1996). POA is generally valid for a particle refractive index close to one, for large scatterers and for small scattering angles, which is the case for the RBC under study. It is based on the vectorial Kirchhoff integral (Jackson 1975) in which the field scattered by a particle is expressed as a function of the electromagnetic field on the particle surface. The relation is rigorous and the approximation consists of attributing a physically suitable value to that unknown surface field. The Fresnel laws and the Poynting theorem have been chosen for this purpose. POA contains anomalous diffraction and Fraunhofer diffraction (Ravey and Mazeron 1982) and can be reduced at will to either. It is therefore more general. Unlike anomalous diffraction and Fraunhofer diffraction, it can handle depolarization effects and explain dissymmetry appearing in small-angle light-scattering (SALS) patterns.

Using POA, we have shown that the above patterns were actually compatible with a description in terms of ellipsoid scatterers for RBC (Mazeron et al., submitted for publication in Biorheology), at least as far as the angular positions of the first two intensity extrema in the NS (north-south) and WE (west-east) directions of the pattern are concerned. In particular, the scatterer dimensions deduced from SALS analysis agree fairly well with those obtained by other methods (Sutera et al. 1989; Tran-Son-Tay 1987); RBC deform at constant surface and the angle between their long axis and the streamlines is small whatever the shear stress. From this point of view, the model of the ellipsoidal scatterer is satisfactory. However it cannot explain the angular repartition of intensity along a ring. Indeed, if we look carefully at the patterns, we notice intensity reinforcement in the rings, neither equatorial nor polar (Fig. 1). They are located at γangles around ±70° with respect to the WE line of the pattern (the WE line and the NS line correspond to $\gamma = 0°$ and $\gamma = 90°$, respectively). In other words the rings are not isointensity curves. Is it possible to use this extra information to characterize more accurately the properties of the scatterers? This is the main point of this paper.

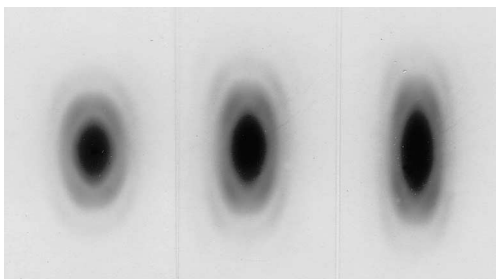

Fig. 1 Experimental SALS patterns of erythrocytes deformed in a viscous flow at increasing shear stresses (30, 40, 190 dynes/cm^2, respectively)

Interpretation and discussion

Some SALS patterns for various shear stresses are presented in Fig. 1 and the fourth-order symmetry can be noticed. They were obtained with human RBC suspensions diluted in Dextran T500 and phosphate-buffered solution (300 mOsm/l, pH = 7.4, viscosity 32 cp at 22 °C, refractive index 1.347). The low-power He-Ne laser beam was perpendicular to the streamlines of the Couette flow.

The theoretical SALS patterns are drawn according to POA by computing the far scattered intensities in all directions defined by the usual scattering angles θ (between scattering and incident directions), and γ (between the scattering plane and the horizontal plane).

The important parameters to be considered in this single scattering problem are: Refractive index, size, orientation, possible distribution laws, structure, and shape of the scatterers. What is the influence of these various factors on the appearance of SALS patterns?

1 Size and refractive index

By using two different radiations of a He-Ne laser ($\lambda = 0.6328$ micron for red light and $\lambda = 0.5431$ micron for green), we can gain some insight into the influence of these two parameters. Indeed, in red light RBC can be considered as dielectric particles whose relative refractive index m is in the range 1.05–1.065 (Streekstraa et al. 1993; Mazeron and Muller 1996; Reynolds et al. 1976). In green light, they are absorbing particles (since erythrocytes are red, they absorb in the green) and thus the imaginary part of m cannot be neglected. In addition their apparent size is larger in green light because size parameters vary as λ^{-1}.

The afore-mentioned reinforcements are visible on the experimental patterns when green light or red light is used. Consequently, it seems that they cannot result from size or refractive index effects. This point has been checked by computing theoretical images according to POA, for an m range characteristic of most biological particles ($1.0 < m < 1.1$) and also for perfectly absorbing particles ($m \to \infty$). The image aspect changes more or less, but the expected reinforcements do not appear. Figure 2 shows some such theortical images corresponding to RBC under shear illuminated by red laser light (top) and by green light (bottom). For green light RBC appear larger than for red light: more rings are then visible on the pattern and its central spot is smaller than in the red. Likewise, for a given m value ($m = 1.065$) we have scanned different size parameters. Intensity reinforcements are never obtained.

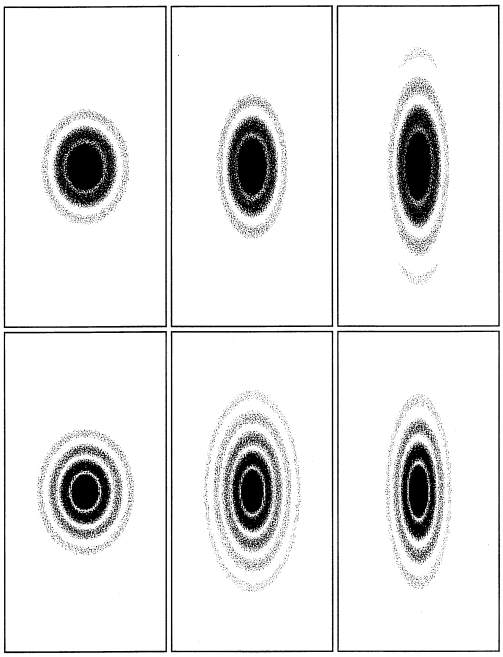

Fig. 2 Theoretical SALS patterns of ellipsoidal particles of the same volume (85 μ^3) but more and more flattened and elongated by a viscous flow. *Upper row:* dielectric particles (m = 1.065). *Lower row:* perfectly conducting particles ($m \to \infty$)

2 Orientation

The constrained RBC shape is supposed to be ellipsoidal with the ellipsoid oriented in the following way (Fig. 3): The major semiaxis b is in the horizontal plane made by the incident light direction and the unperturbed flow direction, tilted by some angle α to the streamline; the medium semiaxis a is perpendicular to this plane in order to minimize the torque exerted on the cell by the flow; the minor semiaxis c characterizes the cell half-width when $\alpha = 0$.

Theoretical SALS patterns computed for $\alpha = 0°$, for $\alpha = 20°$ in the vertical plane and for $\alpha = 20°$ in the horizontal plane, respectively, are presented in Fig. 4. No intensity reinforcement is noticed. For the first 20° orientation, the NS axis pattern is no longer vertical, and for the second the pattern becomes slightly dissymmetric with respect to its NS axis. For other more general orientations in which Euler's angles are not zero, these two effects combine: The fourth-order symmetry of the pattern is lost and the vertical orientation of the pattern disappears. Because the experimental patterns exhibit no apparent dissymmetry and have their NS line vertical, we can state that the reinforcements are not the consequence of an orientation effect. In agreement with earlier observations (Trans-Son-Tay, 1987), the long ellipsoid axis is probably oriented along or nearly along the streamlines. Angle α is certainly small enough so that it cannot markedly influence the shape of the SALS patterns.

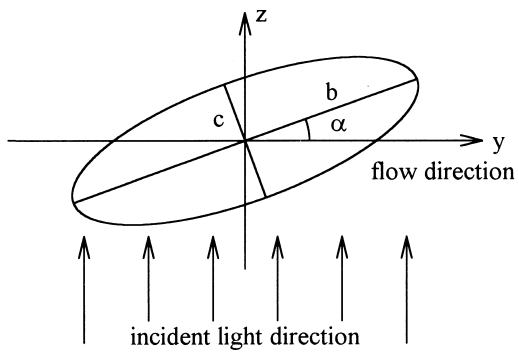

Fig. 3 Ellipsoid orientation with respect to incident light direction z and unperturbed flow direction y. Scattering direction is determined by angle θ with z axis and angle γ with the horizontal plane (y, z)

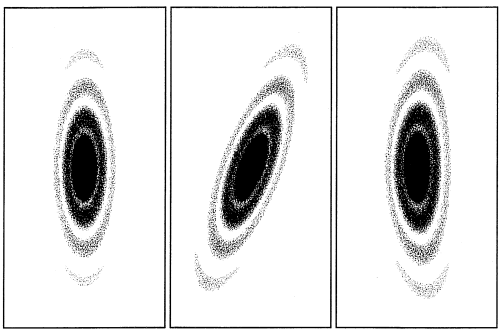

Fig. 4 Theoretical SALS patterns computed according to POA for ellipsoidal RBC. The first image is for $\alpha = 0°$. The long axis was given a 20° inclination to the streamlines in the vertical plane (second pattern) or in the horizontal plane (third pattern). In the first case the NS axis of the pattern is rotated, and in the second a slight but visible dissymmetry appears. Neither could be experimentally observed

3 Distribution laws

By introducing in the POA fortran codes for various probability laws of a Gaussian nature for the size of the scatterers, their orientation, and their refractive index, the preexisting monodispersity decreases or disappears. Generally, the effect is to make the patterns less contrasted without provoking any intensity reinforcements. The patterns become more uniform instead. This hypothesis must then be discarded. As a matter of example, the curves of Fig. 5 show the angular intensity variations versus θ for $\gamma = 0°$ (lower curves) and $\gamma = 90°$ (upper curves), which the probability law (bold lines) and without (plain lines). The effect is striking. With the probability law, the differences between two consecutive intensity maxima and minima are greatly reduced. The pattern sharpness is then lowered. In the limit of random orientation the patterns would become blurred.

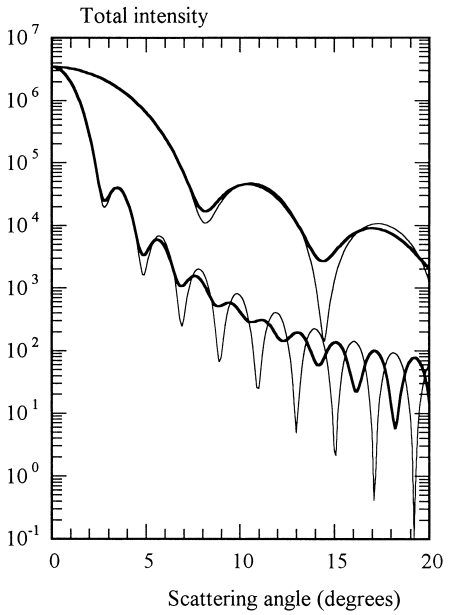

Fig. 5 Plain curves: Angular scattering of a single RBC (volume: 85 μ^3, orientation: $\alpha = 0°$, size parameters: a = 30, b = 90, c = 18, refractive index: 1.065), for $\gamma = 0°$ (*lower curves*) and for $\gamma = 90°$ (*upper curves*). *Bold curves:* idem for a cell population with the same characteristics but whose volumes are normally distributed ($V_{mean} = 85\ \mu^3$, standard deviation = 12.75 μ^3). In this last case the oscillations are greatly diminished

4 Structure

RBC are surrounded by a thin membrane of approximately 70 Å whose refractive index is larger than that of the cell interior. Although this is not simple, it is possible to account for this inhomogeneous structure in POA. As reported above, the approximation requires the knowledge of the electromagnetic field at the surface of the scatterer. Adding a thin refringent membrane modifies this field. Its new value is determined through the use of reflection and transmission coefficients, by considering that the membrane behaves locally like a multiple wave interferometer. The computed results show that this modification neither changes the shape of the SALS patterns nor makes the reinforcements appear.

5 Shape

We pointed out that the three-axis ellipsoid shape was compatible with the experimental patterns obtained, at least as far as the angular positions of the two first extrema in the NS and WE directions are concerned. Therefore, it would be better not to depart too much from this model. Microphotographs of RBC deformed in a rheoscope at higher shear rates (Sutera 1987; Fischer 1980) as well as Fourier transform properties in diffraction, strongly suggest particles with more or less thinned extremities.

To build such a shape, a possible way of proceeding is to consider two ellipsoids with the same center, with the same a and c axes, and with different major axes, b_1 and b_2. Their surface equations are arbitrarily combined according to the following expression:

$$x^2/a^2 + (y^2/b_1^2)\, f(N,x,z) + (y^2/b_2^2)\,[1 - f(N,x,z)] + z^2/c^2 = 1$$

in which

$$f(N,x,z) = \cos^N[(\pi/2)\,(x^2/a^2 + z^2/c^2)^{1/2}]$$

For f = 1 this equation reduces to the first ellipsoid equation and to the second for f = 0. Now for $0 < f < 1$ an intermediate surface between the two ellipsoids is generated. Its shape can be changed at will according to the arbitrary expression taken for function f. By choosing a cosine to the Nth power of some other function, the desired surfaces are obtained. Figure 6 shows (bold outlines) how the particle shape is changed when N increases from 0 to 5. For N = 0 and then f = 1, the undeformed ellipsoid (here the outer) whose semi-axis is b1, is obtained. This is the reference ellipsoidal shape we want to deform into an ellipsoid-like particle with thinned extremities. The extremity thinning can be characterized in the following way: let S(y = b2, N) be the cross sectional area of the particle in the plane perpendicular to y at y = b2. A thinning parameter, ρ, is arbitrarily defined by

$$\rho = 1 - \sqrt{\frac{S(y=b2,\,N)}{S(y=b2,\,N=0)}}$$

For N = 0 the particle is the undeformed reference ellipsoid and $\rho = 0$ (no thinning). When N increases, the thinning is more and more important because the cross sec-

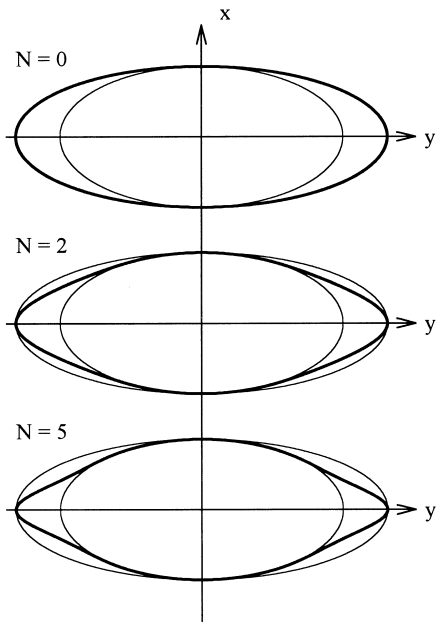

Fig. 6 Shapes generated (*bold curves*) from the two given ellipsoids (*plain curves*) according to N values. For N = 0, the particle is the outer undeformed ellipsoid whose longest semi-axis is b_1. For N increasing, it becomes thinner. For N = 10 (not shown), the particle is like a lemon. For higher N values it tends to the inner ellipsoid whose semi-axis is b_2

tional area is smaller and smaller and ρ increases. Its asymptotic value for $N \to \infty$ is $\rho = 1$.

To compute the corresponding theoretical SALS patterns, it is still necessary to use an approximation. It would be rather difficult to theorize and to use POA for such shapes. The more easily handled anomalous diffraction (Van de Hulst 1957) has been chosen. In fact, it happens that for axial orientation, for small scattering angles ($\theta < 20°$) and for a relative refractive index of the particle not very far from unity, POA and anomalous diffraction lead to nearly the same results. This is due to the geometrical (large dimensions) and optical parameter values ($n = 1.065$) implied in the current problem and by no means a general rule. The anomalous diffraction approximation when applied to undeformed ellipsoids is then unable to explain the intensity reinforcements. What is changed when it is applied to thinned ellipsoids?

We are interested in the first ring, that is, in the first intensity maximum encountered for various γ values. The computed angular intensity curves presented in Fig. 7 are related to a deformed ellipsoid whose thinning parameter is 0.44. They show that for the first intensity maximum, the scattered intensity is maximum for $\gamma = 70°$. In the $\gamma = 90°$ direction, the intensity undergoes an approximately 3.5-fold decrease with respect to this maximum and a still more important decrease in the $\gamma = 0°$ direction. In other words the ring will not be an isointensity curve: It is "open" in the vicinity of $\gamma = 0°$ and 90°, and maximum in intensity in the 60° – 70° zone.

To understand how the intensity reinforcement arises, to ratio $I(\gamma = 70°)/I(\gamma = 90°)$ is studied as a function of the thinning parameter ρ (Fig. 8). For an undeformed ellipsoid ($\rho = 0$), this ratio is unity. As soon as the particle thinning begins (ρ increases), the above ratio strongly increases, indicating an intensity reinforcement in the direction $\gamma = 70°$. This reinforcement is maximum (therefore clearly noticeable on the patterns) for $\rho = 0.36$, which corresponds to N = 3. The particle characteristics are m = 1.065, a = 40, b1 = 85, b2 = 60, c = 19. The volume, V, and the membrane area, S, depend on N and have (computed) values currently encountered in this kind of problem: $V = 90\ \mu^3$, $S = 127\ \mu^2$ for N = 2 and $V = 85\ \mu^3$, $S = 120\ \mu^2$ for N = 5. They are not critical to the phenomenon because reinforcements appear for a large range of size parameters, both experimentally (see experimental patterns) and theoretically. What is important is the thinning of the particle.

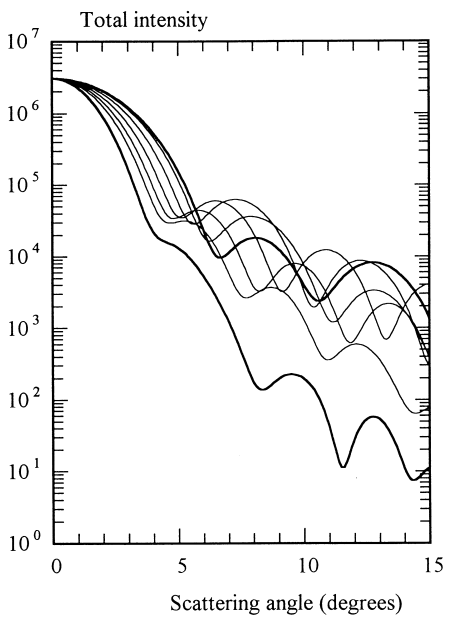

Fig. 7 Example of theoretical angular scattering, according to the anomalous diffraction, of a moderately deformed RBC with thinned extremities (m = 1.065, a = 40, b1 = 85, b2 = 60, c = 19, N = 5, thinning parameter $\rho = 0.44$, volume = 85 μ^3, area = 120 μ^2). From bottom to top: $\gamma = 0°$ (bold), $\gamma = 40°$ to 90° (bold) by steps of 10°. The intensity of the first maximum is maximum for $\gamma = 70°$ and $\theta = 7.3°$

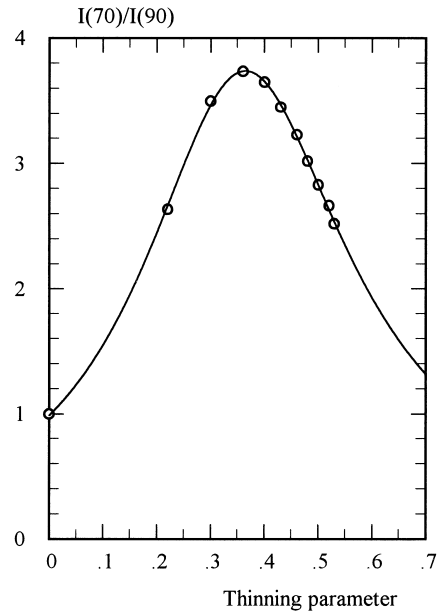

Fig. 8 The ratio $I(\gamma = 70°)/I(\gamma = 90°)$ versus thinning parameter ρ for the scatterer of Fig. 7. As soon as the ellipsoid is thinned (ρ increases), the intensity reinforcement arises at $\gamma = 70°$. The same curve is obtained for $\gamma = 60°$ or neighboring angles

Theoretical SALS patterns of thinned ellipsoids are presented in Fig. 9 (left patterns for N = 2 and right pattern for N = 5, respectively). Their general aspect is nearly the same as that obtained from a true ellipsoid shape with regard to ring angular positions, but what is important is that they exhibit the expected reinforcements. The scatterer shapes considered (i.e., thinned ellipsoids) therefore explain the appearance of the experimental SALS patterns. Such an experimental pattern is presented between the two theoretical ones in Fig. 9. It corresponds to RBC (measured volume 85 μ^3) highly deformed in a shear flow. The agreement is fairly good.

Note that the scatterer shape considered is not purely theoretical: it is close to that displayed by experimental photographs obtained with a rheoscope (Tran-Son-Tay 1987, Fig. 1; Fischer 1980, Fig. 1). It would be interesting to know if, and under which conditions, theoretical mod-

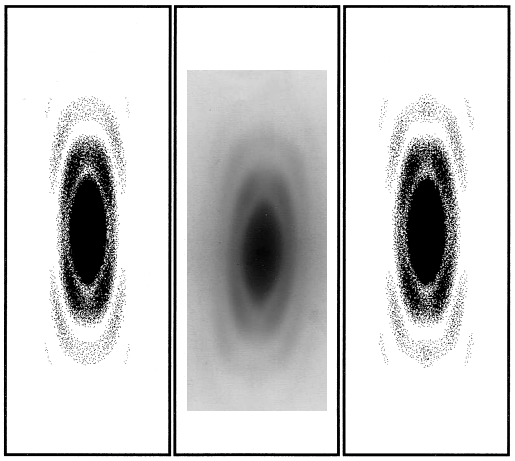

Fig. 9 *Left* and *right:* Theoretical SALS patterns calculated according to the anomalous diffraction for thinned ellipsoids and for N = 2 and 5, respectively. *Middle:* experimental SALS pattern of RBC highly deformed in a simple shear flow (measured RBC volume: 85 μ^3, shear stress >100 dynes/cm^2). They agree fairly well

els based on vesicle dynamics (Kraus et al. 1996) can predict such ellipsoid-like shapes for RBC submitted to a simple shear flow.

Conclusion

The deformation of RBC in a shear flow has been studied by purely light scattering measurements. To this end, the physical optics approximation and the anomalous diffraction have been used. The deformations undergone by RBC are compatible with a description in terms of a nearly ellipsoid shape: Ellipsoid extremities are slightly thinned.

This conclusion has been made possible because we have been interested in elements other than the central spot in the experimental patterns. Indeed, the study of the location of satellite stains is equivalent to the comparison of scattered intensity levels. With the help of suitable scattering theories, the exploitation of this extra information permits some improvement in the knowledge of the properties of the scatterers. It plays a role too, as we have seen, in the discrimination beween several different hypotheses.

References

Barber P, Hill S (1990) Light scattering by particles: computational methods. World Scientific Publishing Co Pte Ltd, Singapore New Jersey London Hong Kong

Barthes-Biesel D (1980) Motion of a spherical microcapsule freely suspended in a linear shear flow. J Fluid Mech 100: 831–853

Bessis M, Mohandas N, Feo C (1980) Automated ektacytometry: a new method of measuring red cell deformability and red cell indices. Blood Cells 6:315–327

Brennen C (1975) A concentrated suspension model for the Couette rheology of blood. Can J Chem Engng 53:126–133

Brenner H, Bungway P (1971) Rigid particle and liquid-droplet models of red cell motion in capillary tubes. Fedn Proc Fedn Socs Exp Biol 30:1565–1576

Draine B, Flatau P (1993) Discrete-dipole approximation for scattering calculations. J Opt Soc Am A 11:1491–1499

Fischer T (1980) On the energy dissipation in a tank-treading human red blood cell. Biophys J 32:863–868

Fischer T, Stohr M, Schmid-Schönbein H (1978) Red blood cell (RBC) microrheology: comparison of the behavior of single RBC and liquid droplets in shear flow. A I Ch E Symp Series no 182, 74:38–45

Fischer T, Schmid-Schönbein H (1977) Tank-tread motion of red cell membranes in viscometric flow: behavior of intracellular extracellular markers. Blood Cells 3:351–365

Gauthier F, Goldsmith H, Mason S (1972) Flow of suspensions through tubes-X Liquid drops as models of erythrocytes. Biorheology 9:205–224

Goldsmith H (1967) Microscopic flow properties of red cells. Fedn Proc Fedn Am Socs Exp Biol 26:1813–1820

Goldsmith H, Marlow J (1967) The microrheology of dispersions. In: Eirich FR (Ed) Rheology, theory and applications. Academic 4:85–250

Goldsmith H, Marlow J (1972) Flow behavior of erythrocytes. I Rotation and deformation in dilute suspensions. Proc R Soc Lond B1 82:351–384

Guerlet B, Barthes-Biesel D, Stoltz J (1977) Deformation of a sphered red blood cell freely suspended in a simple shear flow. Cardiovascular Pulmonary Dynamics INSERM 71:257–264

Jackson JD (1975) Classical electrodynamics. Wyley, New-York, p 432

Keller S, Skalak S (1982) Motion of a tank-treading ellipsoidal particle in a shear flow. J Fluid Mech 120:27–47

Kline K (1972) On a liquid drop model of blood rheology. Biorheology 9:287–299

Kraus M, Wintz W, Seifert U, Lipowsky R (1996) Fluid vesicles in shear flow. Phys Rev Lett 77:3685–3688

Mazeron P, Muller S (1996) Light scattering by ellipsoids in a physical optics approximation. Appl Opt 35:3726–3735

Ravey JC, Mazeron P (1983) Light scattering by large spheroids in the physical optics approximation: numerical comparison with other approximate and exact results. J Opt (Paris) 14:29–41

Reynolds L, Johnson C, Ishimaru A (1976) Diffuse reflectance from a finite blood medium: applications to the modeling of fiber optic catheters. Appl Opt 15:2059–2067

Richardson E (1974) Deformation and haemolysis of red cells in shear flow. Proc R Soc Lond A 338:129–153

Schmid-Schönbein H, Wells R (1969) Fluid drop-like transition of erythrocytes under shear. Science 165:288–291

Streekstra G, Hoekstra A, Nijhof E, Heethar R (1993) Light scattering by red blood cells in ektacytometry: Fraunhofer versus anomalous diffraction. Appl Opt 32:2266–2272

Streekstra G, Hoekstra A, Heethaar R (1994) Anomalous diffraction by arbitrarily oriented ellipsoids: applications in ektacytometry. Appl Opt 33:7288–7296

Sutera S, Pierre P, Zahalak G (1989) Deduction of intrinsic mechanical properties of the erythrocyte membrane from observations of tank-treading in the rheoscope. Biorheology 26:177–197

Tran-Son-Tay S, Sutera S, Zahalak G, Rao P (1987) Membrane stress internal pressure in a red blood cell freely suspended in a shear flow. Biophys J 51:915–924

van de Hulst HC (1957) Light scattering by small particles. Wiley, New York

Zahalak G, Sutera S (1981) Fraunhofer diffraction of an oriented monodisperse system of prolate ellipsoids. J Colloid Interface Sci 82:423–429